Optimization of planar LIF/Mie imaging for droplet sizing characterization of dilute sprays

Sébastien Garcia, Pierre Doublet, Christine Lempereur, Geoffroy Illac, M. Stiti, E. Berrocal, Mikael Orain

Experiments in Fluids (2023) 64:165
https://doi.org/10.1007/s00348-023-03706-8

RESEARCH ARTICLE

Optimization of planar LIF/Mie imaging for droplet sizing characterization of dilute sprays

S. Garcia[1] · P. Doublet[1] · C. Lempereur[1] · G. Illac[1] · M. Stiti[2] · E. Berrocal[2] · M. Orain[1]

Received: 28 March 2023 / Revised: 8 September 2023 / Accepted: 11 September 2023 / Published online: 2 October 2023

Abstract
The aim of this work is to investigate the planar LIF/Mie droplet sizing technique from an experimental and theoretical point of view. This technique is a good alternative compared to point measurements (e.g., phase Doppler anemometry) or integral approaches (e.g., laser diffraction). It allows measurement of the Sauter mean diameter over a wide field, providing the spray topology and droplet size in a limited amount of time. Nevertheless, its implementation remains challenging due to the fact that the usual assumptions underlying the technique are not fully valid in practice. To overcome these limitations, an innovative experimental set-up has been developed including the use of a telecentric lens and a TwinCam beam splitter device. The benefit of the key optical elements introduced in the set-up will be discussed and quantified in the paper. In particular, it is shown that the telecentric lens removes angular dependency of the Lorenz–Mie optical signals. This is demonstrated using an ethanol hollow cone spray (seeded with rhodamine 6G) generated from a simplex injector at atmospheric pressure and ambient room temperature. A calibration procedure, based on phase Doppler anemometry measurements, is used to convert the LIF/Mie into Sauter mean diameter maps. The optical depth of the spray has been measured, exhibiting values less than 0.4 (equal to 67% light transmission), which corresponds to a dilute cloud of droplets where multiple light scattering is not an issue. These effects have been quantified using Monte Carlo simulations. Finally, a study of the injection parameters has been undertaken, showing the robustness and efficiency of the planar LIF/Mie droplet sizing method to obtain two-dimensional maps of the Sauter mean diameter.

1 Introduction

According to Rayleigh (1878), a spray can be defined as a collection of droplets in a gaseous medium. It results from the atomization of the liquid, which represents a disintegration process. In gas turbines, the injection of liquid fuel into the highly turbulent gas flow of a combustion chamber gives rise to many complex physical phenomena: the liquid stream is stretched into ligaments and atomized into droplets that are then transported further downstream, while evaporating and enabling the combustion process. Fine atomization is required to promote vaporization and combustion of sprays. Most of the time, sprays are characterized by their shape and droplet size distribution. The droplet size distribution of a hollow cone spray, used in aeronautical engines, extends from a few microns to several hundred microns. Typically, a graphical representation of droplet size distribution is given through a histogram based on the number and/or volume of particles (Lefebvre and McDonell 2017). However, in order to facilitate calculations related to mass transfer and flow processes, Mugele and Evans (1951) have established a standardized notation of mean diameters (instead of the use of a complete droplet size distribution):

$$D_{ab} = \left[\frac{\sum N_i D_i^a}{\sum N_i D_i^b} \right]^{1/(a-b)} \quad (1)$$

In the case of two-phase combustion applications, the aim is to obtain a spray with a maximum exchange surface in order to increase the exchanges between the phases (especially evaporation) for a given volume of liquid. The Sauter mean diameter (SMD or D_{32}) is classically used to characterize injection systems in gas turbines (Lefebvre and McDonell 2017). The SMD is an important quantity for mass transfer processes: a small SMD indicates fine

✉ S. Garcia
sebastien.garcia@onera.fr

[1] ONERA/DMPE, Toulouse University, 31055 Toulouse, France

[2] Division of Combustion Physics, Department of Physics, Lund University, Lund, Sweden

evaporation, weak penetration and efficient mixing and combustion processes. The application of CFD codes to technical sprays is still challenging (Sanjosé et al. 2011; Hervo et al. 2018): in fact, if numerical parameters need to be tuned to fit experimental results, these data must in turn be reliable. In this respect, experiments yield essential information for the development and evaluation of atomization and spray flow models.

In order to fulfill the accuracy requirement, laser-based optical diagnostics are in steady progress (Berrocal et al. 2023). Although a conventional pointwise technique, phase Doppler anemometry (PDA), has been widely investigated over the last few decades, whole-field measurement techniques are promising means to reduce test duration and cost. In this context, the planar LIF/Mie technique, also called planar droplet sizing (PDS), is a laser imaging method originally proposed by Yeh et al. (1993) and used to obtain SMD distribution in sprays. This technique is based on the detection of the Lorenz–Mie scattering signal (Mie) and the laser-induced fluorescence (LIF) emission from droplets illuminated with a laser beam. Mie scattering is essentially based on the phenomenon of elastic light scattering by spherical particles. The mathematical solutions are given by the Lorenz–Mie theory (Lorenz 1890; Mie 1908). In this theory, for droplets whose diameter is larger than the emission wavelength, the scattered intensity is proportional to the square diameter of the particles. Laven (2008) has developed a computer program, known as "MiePlot," for the calculation of scattered light from a sphere using Mie theory and the Debye series. MiePlot was originally designed to provide a simple interface, using the conventional BHMIE algorithm, as published by Bohren and Huffman (1983). The input data for this code are the real (n) and imaginary (k) refractive index, the laser excitation wavelength (λ), the scattering angle (α), the laser polarization (S-pol, P-pol or Unpolarized), and the diameter range of the droplet (D) (monodisperse or polydisperse distributions). Unlike Mie scattering, the LIF signal is based on inelastic light emission (the fluorescent emission is at a longer wavelength than the excitation wavelength). When the laser crosses the spray, droplets absorb the incident light and spontaneously restore that energy via inelastic light emission. However, fluorescence is only achieved if the liquid contains fluorescent molecules. If no fluorophores are naturally present in the liquid, it must be seeded with a fluorescent dye. According to Felton et al. (1993), the LIF signal is proportional to the fluorescent molecule concentration and depends on liquid volume. Consequently, fluorescence emission from droplets is proportional to their cubic diameter. The LIF/Mie technique consists in acquiring two images of a spray, in two different spectral ranges by applying a set of optical filters. According to Sankar et al. (1999), all the light collected by each pixel of the camera, during the acquisition time, correspond to the sum of the scattered light and fluorescent emission from all the droplets that have crossed the measurement volume. Therefore, for an image with coordinates x and y, the scattered and fluorescent intensities correspond to:

$$I_{\mathrm{s}}(x,y) = I_{\mathrm{i}}(x,y)C_s \sum N_i(x,y)D_i^2(x,y) \tag{2}$$

$$I_{\mathrm{f}}(x,y) = I_{\mathrm{i}}(x,y)C_f \sum N_i(x,y)D_i^3(x,y) \tag{3}$$

where $I_{\mathrm{i}}(x,\mathrm{y})$ is the incident intensity, $I_f(x,y)$ and $I_s(x,y)$ are, respectively, the fluorescent and the scattered light intensities, N_i is the number of particles with diameter D_i, and C_f and C_s are proportionality coefficients that can be defined experimentally. The ratio of both images is therefore proportional to the SMD of the size distribution of the N measured droplets:

$$\frac{I_{\mathrm{f}}(x,y)}{I_{\mathrm{s}}(x,y)} = \frac{C_f}{C_s}\left[\frac{\sum N_i(x,y)D_i^3(x,y)}{\sum N_i(x,y)D_i^2(x,y)}\right] \tag{4}$$

Also:

$$\frac{I_{\mathrm{f}}(x,y)}{I_{\mathrm{s}}(x,y)} = \frac{C_f}{C_s}D_{32}(x,y) = \mathrm{K}D_{32}(x,y) \tag{5}$$

The first applications of this technique for the droplet sizing of industrial sprays have been carried out by Le Gal et al. (1999), Jermy and Greenhalgh (2000) or even Stojkovic and Sick (2001). Afterward, Domann and Hardalupas (2001, 2003) and Charalampous and Hardalupas (2011a, b) have conducted extensive research on the PDS technique, in order to determine its limitations. Regarding the LIF intensity, the authors show that the relationship between droplet volume and fluorescence intensity depends on the dye concentration. Low dye concentration results in a closer proportionality to volume, while significant deviation can be observed for large dye concentrations. Moreover, in the event of evaporation or combustion, this concentration changes, as well as the quantum yield and the molar absorptivity, which are temperature-dependent. In this case also, vapor and liquid phases cannot be separated in the fluorescence signal, which degrades the sizing accuracy of the technique. Optimization of the scattering angle as a function of the refractive index of the liquid is also proposed; a forward scattering direction at 60° is recommended to make the Mie intensity proportional to the droplet surface area (Charalampous and Hardalupas, 2011).

Laser imaging can be reliably quantitative when performed in low-density sprays where single light scattering predominates. However, in optically dense sprays corresponding to optical depth OD > 1, additional scattering events occur in the spray environment prior to reaching the camera sensor. As a result, without the suppression of the

multiple light scattering intensity, a reliable SMD mapping cannot be acquired. To solve this issue, an imaging method known as structured laser illumination planar imaging (SLIPI) has been developed by the Physics Department at Lund University (Berrocal et al. 2008). Several implementations of SLIPI image reconstruction have been developed by Kristensson et al. (2010a, b), Mishra et al. (2014, 2017a, 2017b). These techniques are based on Fourier filtering and phase-shifted image acquisition. The literature also contains numerical studies of the phenomenon of multiple diffusion (Jermy and Allen (2002), Berrocal (2006)). To perform an analysis of multiple scattering, a software called "Multi-Scattering" has been developed by Jönsson and Berrocal (2020) and validated by Frantz et al. (2022). The model is based on the use of the Monte Carlo (MC) method, where billions of photon packets are tracked via simulation, while propagating in scattering and/or absorbing media. This software can be used before applying any quantitative laser imaging techniques, to determine if SLIPI is required in the experimental set-up, like a decision-making tool.

This paper is dedicated to the droplet size characterization of a hollow cone spray by applying the LIF/Mie technique with an innovative optical set-up based on the use of a camera telecentric lens and a fully integrated beam splitter device. This removes several sources of uncertainty observed with traditional set-ups: conventional lens and filter wheel (Yeh et al. 1993; Le Gal et al. 1999). The remainder of the paper comprises four sections. A description of the injection systems and the actual implementation of the technique is presented in the first section. In the second section, the optical conditions are defined and a multiple scattering analysis is performed with the "Multi-Scattering" software in order to quantify any undesired effects from multiple light scattering. The third section is dedicated to investigating the parameters that influence the accuracy of the LIF/Mie technique. The essential use of a telecentric lens will be demonstrated in this section using MiePlot simulations. The final section is dedicated to experimental results obtained with a simplex injector. First, we detail the calibration procedure, based on PDA measurements, which is used to convert the LIF/Mie into SMD maps. A parametric study is conducted to determine the influence of the injection pressure on SMD, which demonstrates the potential of the LIF/Mie technique for further industrial applications. The paper ends with a summary of the results and perspectives.

2 Experimental set-up

2.1 Injection system

The injection system is an industrial model (Delavan, simplex model, spray aperture of 60°, hollow cone type, Flow

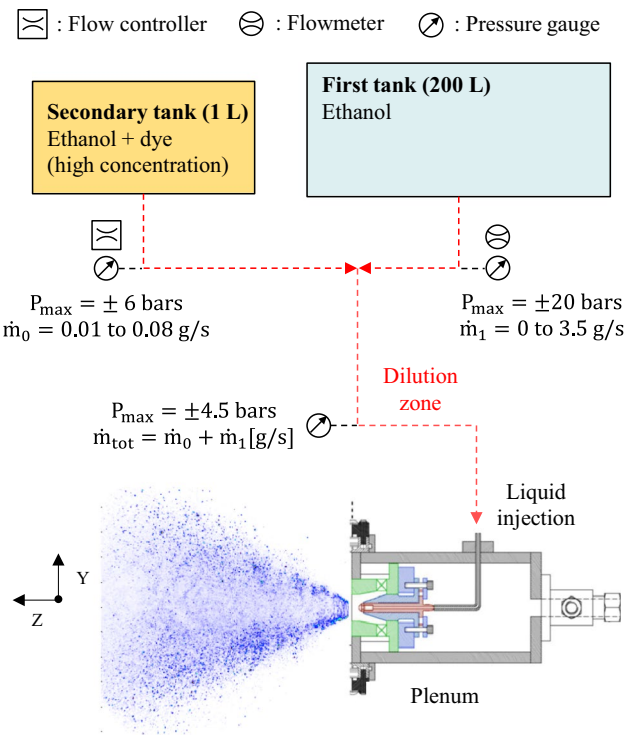

Fig. 1 Scheme of the injection test bench

Number: FN = 5.21 ± 0.02 l·h^{-1}·bar$^{-1/2}$), which produces polydisperse droplets with size in the range (1–150) µm. Experiments are conducted at ambient temperature and atmospheric pressure. The liquid used for the experiments is ethanol for safety reasons and also because its surface tension ($\sigma = 0.0022$ N/m) is close to that of Jet A-1 (kerosene fuel typically used in aeronautics). As previously discussed, the LIF/Mie technique requires a fluorescent liquid to promote the LIF signal and derive SMD maps. According to Ying et al. (2007), ethanol can fluoresce without the addition of a dye. However, ethanol must be excited by an ultraviolet light with a wavelength shorter than 250 nm (the emission bands are centered in the 290–350 nm range). For convenience, a visible laser ($\lambda = 532$ nm) is used for the experiments and a fluorescent dye must be added to the ethanol. Among the potential dyes soluble in ethanol, rhodamine 6G (Rh6G) is the most efficient under the present experimental conditions. Rh6G has a high solubility in ethanol and its temperature dependence is quite low when excited at 532 nm (Chaze et al. 2016). Furthermore, the high quantum efficiency of Rh6G (about 0.95 (Kubin and Fletcher 1982)) and its strong absorption at 532 nm are advantageous for maximizing the fluorescence signal. As seen previously, the dye concentration has a tremendous effect on the LIF signal. As a result, an injection test bench has been designed in order to perfectly control the dye concentration during the measurements (Fig. 1).

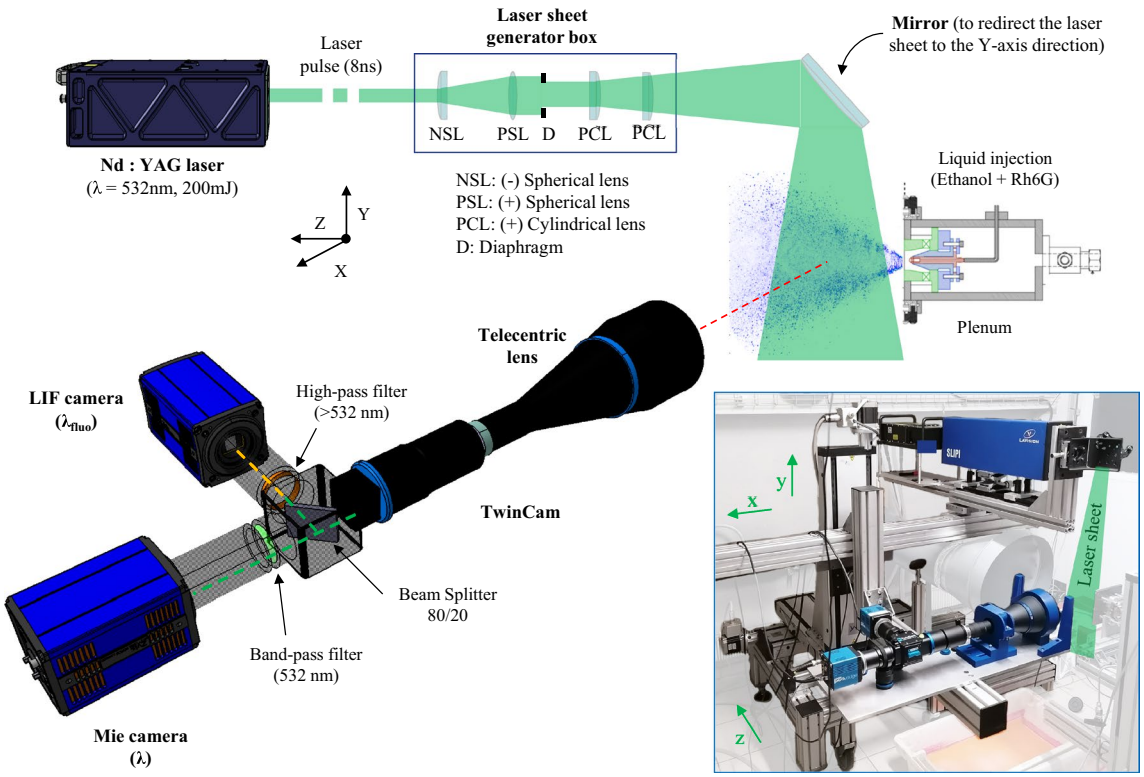

Fig. 2 View of the optical LIF/Mie droplet sizing arrangement

The experimental test bench is composed of two liquid containers: a large 200 L tank containing pure ethanol and a small 1 L tank containing ethanol heavily seeded with Rh6G. Indeed, the large tank cannot be seeded directly because it would cause the pollution of the entire liquid supply line for future experiments. Therefore, a specific supply containing a small volume of seeded ethanol is connected to the main liquid line upstream from the injector. The solution of ethanol and Rh6G is mixed with pure ethanol by means of a Y-junction together with a 2-m-long pipe downstream from the junction, which is enough to ensure proper mixing between the fluids. After dilution, the dye concentration (C_1) in the injector is obtained from the dilution law:

$$C_1 = C_0 \frac{\dot{m}_1}{\dot{m}_0 + \dot{m}_1} \tag{6}$$

where $\dot{m}_1$ is the mass flow-rate from the first tank (pure ethanol), $\dot{m}_2$ is the mass flow-rate from the secondary tank (ethanol seeded with Rh6G) and C_0 is the dye concentration of the secondary tank. The amount of Rh6G in the secondary tank is measured with an analytical balance (Adventurer™ Pro AV114C Ohaus®—resolution: 0.1 mg). To ensure optimum control of the mixture, the pressure is controlled by an analog manometer and the mass flow-rate by a Coriolis flowmeter (Micro Motion) on the 200 L pipeline. On the 1 L pipeline, the pressure is controlled by an analog manometer and the mass flow-rate by a Coriolis flow controller (Brooks instrument). Thanks to this experimental installation, the dye concentration at the outlet of the injector is perfectly controlled and maintained constant throughout the measurement.

2.2 Optical equipment

See Table 1.

2.3 Optical set-up

The LIF/Mie optical set-up is displayed in Fig. 2. For droplet illumination, the beam of a frequency-doubled Nd: YAG—532 nm pulsed laser (No. 1 in Table 1) is formed into a light sheet by a combination of spherical and cylindrical lenses. For space reasons around the injection test bench, the laser source and the lenses must be placed above the spray and a mirror (No. 11 in Table 1) is used to send the laser sheet through the spray. The reception module is placed at a 90° scattering angle. Both conventional (No. 4 in Table 1) and telecentric (No. 5 in Table 1) lenses are compared in the experiments, in order to highlight the benefits of the latter. Two sCMOS cameras (No. 3 in Table 1) are used and connected to the lens by a TwinCam module (No. 7

Table 1 List of optical materials used in the experiments

No.	Details
1	Pulsed laser—Quantel Twins Big Sky (Nd: YAG—532 nm, 200 mJ, 10 Hz, 8 ns impulsion and horizontal polarization)
2	Broad spectrum xenon lamp—ASAHI MAX303
3	Camera—sCMOS PCO.edge 4.2 (2048^2, pixel size: 6.5×6.5 µm^2, 16 bits, max fps 100 fps)
4	Conventional lens—Nikon Micro-Nikkor (Macro-objectif—f = 60 mm—f/2.8 D-AF)
5	Telecentric lens—OPTO Engineering TC1MHR080-C (1/1.2", magnification 0.134x, C mount)
6	Telecentric lens—Edmund Optique 33–096 (2/3", magnification 1x, C mount)
7	TwinCam—CAIRN research
8	High-pass edge filter—Semrock BLP01-532R
9	Band-pass filter—Chroma FWHM (10 nm width) /zet532-10x
10	Beam splitter—Chroma (non-polarizing 80/20)
11	Mirror—Newport (M2: Ø = 50.8 mm)
12	PDA—Dantec Dynamics (FlowExplorer: $\lambda_1 = 532$ nm & $\lambda_2 = 671$ nm)

in Table 1). The latter is used to simultaneously record the LIF and Mie signals in the two cameras. It allows the physical superimposition of optical paths, which eliminates the sources of error typically observed with two cameras recording a scene at different viewing angles. Both cameras have a 24 µs exposure time and are used in a $\times 2$ binning mode to increase the signal-to-noise ratio. The telecentric lens yields a field-of-view of 84×84 mm2 and a spatial resolution of approximately 80 µm/pixel. It should be noted that the main disadvantage of a telecentric lens is its high cost, constant focal length and a large f-number. The conventional lens leads to a field-of-view of 63×63 mm2 and a spatial resolution of approximately 60 µm/pixel. The camera used for LIF measurements is equipped with a specific high-pass edge filter (No. 8 in Table 1), efficiently blocking the laser light (optical density 7 at 532 nm) and high transmission (> 95%) above 541 nm. This ensures that there is no contamination from scattered light at 532 nm in the LIF image acquired by this camera. The camera used for Mie measurements is equipped with a 532 nm band-pass filter (No. 9 in Table 1). Since the LIF signal is significantly lower than the Mie signal, a beam splitter (No. 10 in Table 1) is used to redirect 80% of the collected signal to the LIF camera and 20% to the Mie camera, which is enough to obtain a good LIF signal.

2.4 Acquisition and post-processing

The acquisition and post-processing routine of the images is carried out using a custom-made interface developed on the App Designer from MATLAB®. The mappings presented in this paper are all based on the acquisition and averaging of 800 instantaneous images. Thus, the time required to acquire all the LIF and Mie images is 80 s, which is significantly lower than that of a grid of PDA measurements with the same spatial resolution. In order to remove the influence of the camera offset measured on the results, a "dark image" is acquired and subtracted from each average LIF and Mie image, during the post-processing routine. Then, to define a physical scale on each average image, a calibration is performed with a calibration plate (LaVision 106–10). During image acquisition, the TwinCam system allows a physical superimposition of the optical paths (error: ± 1 px), but during post-processing, the LIF and Mie images are then dewarped and repositioned according to a common origin (error: 0.1 px). The application of the ratio to the whole LIF and Mie images produces an aberrant result outside the spray area, so a mask is defined and applied on the mapping. In addition, an average filtering is performed when applying the ratio to smooth the result, i.e., the value of each pixel is calculated from the mean of three of its neighboring pixels. The development of this acquisition and post-processing interface allows the acquisition and definition of SMD maps in a very short time (a few minutes). Table 2 summarizes all the treatments.

3 Applicability of the measurement technique

For all optical diagnostic techniques, it is necessary to know the geometrical constraints and optical conditions (e.g., optical depth, multiple light scattering) of the spray. The choice of the optical set-up is dependent on these parameters. In this section, an approach is used to define the conditions of application of the LIF/Mie technique.

3.1 Defining the measurement region

The LIF/Mie droplet sizing technique is applicable where the drops are perfectly spherical, i.e., in the spray region and in the last part of the spray formation region, because when you get closer to the injector, liquid bodies have various

Table 2 Different steps of the processing routine

Nos.	Steps
1	Acquisition of 800 instantaneous LIF & Mie images
2	Average
3	Subtraction of the "dark image" on the average images
4	Geometrical calibration of the average images (dewarping and superimposition)
5	Creation of a mask from a threshold on the LIF and Mie images, allowing to limit the calculation to the region of the spray
6	Calculation of the LIF/Mie image
7	Average Gaussian filtering on the ratio image
8	Application of the mask on the ratio image

irregular shapes, including the presence of ligaments. Thus, the separation must be defined. This require a high-resolution visualization of the liquid structures using single-shot imaging. This has been applied using high-resolution planar laser-induced fluorescence (PLIF). It has been shown by Berrocal et al. (2018) and Berrocal et al. (2019) that LIF detection provides several advantages for imaging spray formation region, while elastic scattering is not faithful to the liquid structures. This is due to the fact that elastically scattered light is generated at the liquid/gas interfaces and a collimated beam will have light reflected and refracted to some preferential directions. This creates a number of unwanted artifacts such as glare points and strong reflections responsible to saturation spots on the recorded images. Conversely, the LIF signal generated within the liquid is mostly volume dependent and shows faithful images of the liquid structures as shown in the zooms images of Fig. 3. Also, the use of a compact telecentric lens makes it possible to reduce the contribution of out-of-focus light, because of its short depth-of-field, thus providing more clearly sectioned images. The optical set-up used for PLIF imaging is the same as that represented in Fig. 2 (without the optics for Mie imaging). The compact telecentric lens (No. 6 in Table 1) allows to visualize spray areas of 13.3×13.3 mm^2 with a spatial resolution of 6.5 µm/pixel.

As shown in Fig. 3, the injector is embedded in the combustion chamber dome to a depth of about 3 mm. Therefore, a small part of the liquid cone is not observed. Three atomization regions are illustrated in the close-ups (Fig. 3). In the primary breakup zone, which extends from the back chamber to the first 10 mm, the development of instabilities on the surface of the liquid cone generates ligaments. In this

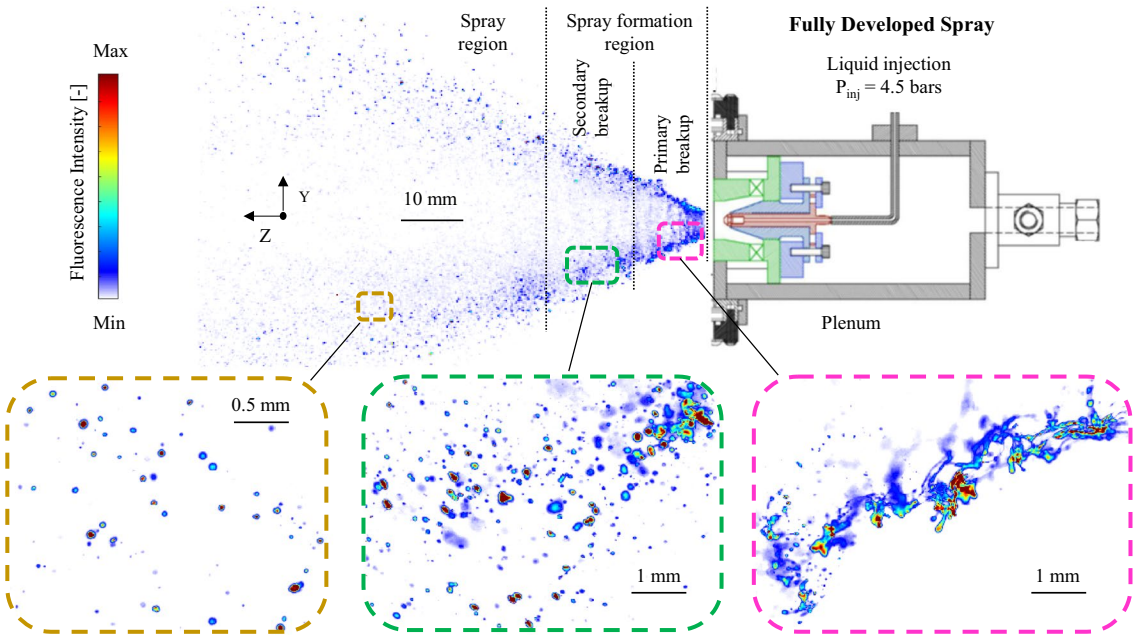

Fig. 3 High-contrast / high-resolution visualization of the ethanol hollow cone spray using the PLIF technique. The different atomization regimes are illustrated in the circles that represent close-ups of the spray

zone, the first large liquid clusters are torn off. However, droplets are not yet formed and, therefore, this spray area cannot be investigated using the LIF/Mie technique. In the secondary breakup zone, which extends from 10 to 20 mm, due to aerodynamic forces, the ligaments have all been disintegrated and replaced by large liquid bodies, most of them with droplet-like shapes. The last region of the spray, beyond 20 mm from the injection point, is the dilute zone where breakup is over and only droplets are present. As a result, in both the latter spray areas, the LIF/Mie technique can be confidently applied, and both fluorescence and scattered light intensities are assumed to be proportional to the intensity of the incident light on the particle. The advantage of the LIF/Mie technique is to eliminate this dependence on the incident intensity, which can vary in the field-of-view due to the inhomogeneity of the laser sheet.

3.2 Multiple light scattering analysis

As previously mentioned, multiple light scattering (more than one order of scattering event) is the major drawback when applying laser planar imaging in sprays. It is related to the density of the spray [#/m^3]: the denser the spray, the more multiple scattering occurs. To estimate multiple scattering, the use of a Monte Carlo software such as "MultiScattering" (Jönsson and Berrocal 2020) makes it possible to define the number of scattering events for a defined optical condition. The implementation of the simulation can be summarized as follows: First of all, photon packets are emitted from a light source. The angular and spatial distribution of the light source can be adjusted depending on the purpose of the simulation (here the interest is to reproduce the illumination of a laser sheet). A measurement volume representative of a part of the spray is then defined. Throughout this volume, the multi-scattering code attempts to solve, via the Monte Carlo method, the Radiative Transfer Equation (RTE):

$$\frac{1}{C}\frac{\partial I(\vec{r},\vec{s},t)}{\partial t} = -\mu_s.I\left(\vec{r},\vec{s},t\right) - \mu_a.I\left(\vec{r},\vec{s},t\right) + \mu_s\int_{4\pi} f\left(\vec{s}',\vec{s}\right).I\left(\vec{r},\vec{s},t\right)\mathrm{d}\Omega' \tag{7}$$

where C is the speed of light, t is time, $\vec{r}$ is the vector position, $\vec{s}$ is the incident direction of propagation, μ_s and μ_a are, respectively, scattering and absorption coefficients and $f\left(\vec{s}\prime,\vec{s}\right)$ is the scattering phase function derived from the appropriate scattering theory (i.e., Lorenz–Mie or Rayleigh-Gans theory). In this equation, the variation of light intensity (I) along an incident direction is due to the loss of intensity by scattering in other directions (first term) and absorption (second term), to which is added the gain in intensity due to multiple scattering (last term). At the end of the calculation, photon paths are tracked within the simulated volume. Random samples are taken from successive probability distributions, which govern various interactions and transitions. Once a photon packet exits the simulated volume, the parameters of interest are extracted from its traveling history. Among these parameters, the intensity profile and the scattering orders can be obtained. These steps are repeated for a large number of photons until sufficient statistics are accumulated (by tracking several billion photons).

In order to solve the RTE, the boundary conditions must be defined through parameters such as the droplet size distribution and the optical properties (i.e., the laser wavelength, refractive index of the liquid and surrounding medium, the scattering and absorption coefficients μ_s and μ_a) of the light transmission (T) are determined by the Beer–Lambert law:

$$T = \frac{I(x)}{I(0)} = e^{-\mathrm{OD}} \tag{8}$$

where $I(0)$ the initial intensity, $I(x)$ the transmitted intensity, and OD the optical depth (also called τ in the literature). During a laser / spray interaction, the OD parameter defines the average number of scattering events that statistically occur when a photon crosses the spray. According to Eq. 8, the initial intensity decreases exponentially over the distance traveled by the laser beam through the spray, giving rise to the extinction phenomenon. Under the hypothesis of a homogeneous low-density medium, OD is defined as:

$$\mathrm{OD} = \mu_e \cdot x = N \cdot \sigma_e \cdot x \tag{9}$$

where μ_e [m^{-1}] is the extinction coefficient, x [m] the distance traveled by the light in the absorbing medium, N [#/m^3] the particle density, and σ_e [m^2] the extinction cross section. The local extinction coefficient μ_e [m^{-1}] is a spray characteristic parameter because it describes the probability of interaction between light and matter per distance unit. From Van de Hulst (1981) and Bohren and Huffman (1983), the extinction concept results from scattering and absorption phenomena of an incident electromagnetic wave crossing a turbid medium. Thus, this signal attenuation phenomenon corresponds to the sum of both contributions: scattering and absorption.

$$\mu_e = \mu_s + \mu_a \tag{10}$$

To carry out the simulation, the boundary conditions mentioned above must be known. The particle size distribution is obtained with PDA measurements (used for the LIF/Mie calibration), the laser wavelength is known, and the refractive index depends on the liquid used, but no information on the transmittance of the medium is available. To determine the transmittance of the studied spray, several experimental measurement techniques based on the

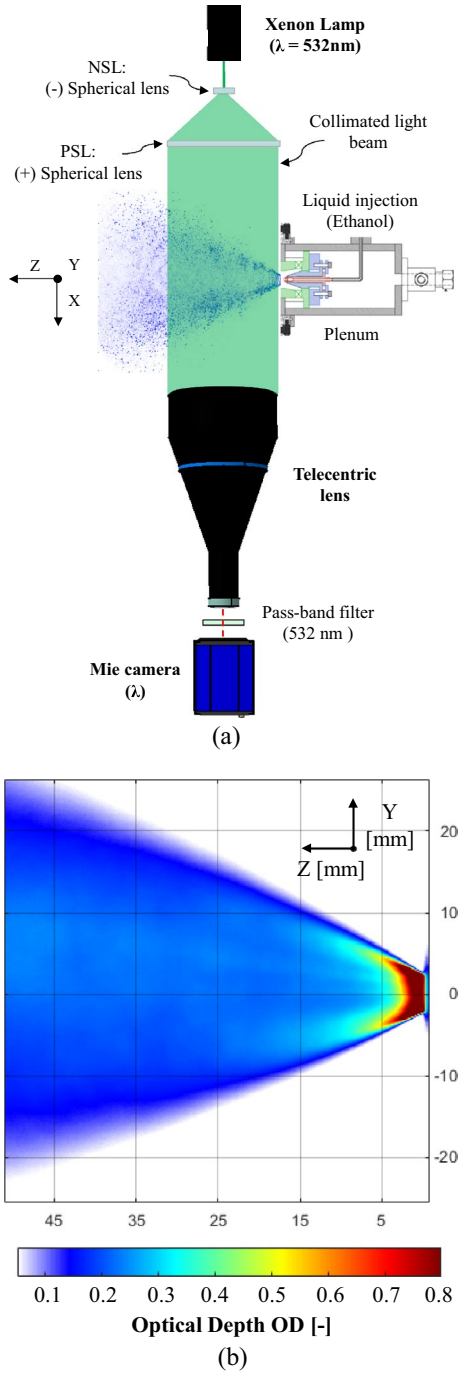

Fig. 4 **a** Experimental set-up used to measure mean transmission through the spray **b** Average OD mapping (500 instantaneous images considered) of the ethanol hollow cone spray (without Rh6G), obtained for a maximal injection pressure value of 4.5 bars

Beer–Lambert law (Eq. 8) are cited in the literature (Kristensson et al. (2011), Wellander et al. (2011), Stiti et al. (2022)). The simplest technique to implement is described by Stiti et al. (2022), where an integral measurement is realized through the spray and allows an OD map to be obtained.

3.2.1 Optical depth measurements

The experimental set-up used to measure the OD is presented in Fig. 4a. Two spherical lenses and a low-divergence broadband-spectrum xenon lamp (No. 2 in Table 1) filtered at 532 nm are used to generate a collimated light beam diameter of approximately 12 cm. The detection is composed of a sCMOS camera (No. 3 in Table 1) connected to a large telecentric lens (No. 5 in Table 1) equipped with a 532 nm band-pass filter (No. 9 in Table 1). The experimental procedure is as follows: image acquisition is first realized without spray injection, in order to determine the maximum incident intensity on each pixel of the camera ($I(0)$ in Eq. 8). Image acquisition is performed with spray injection, to determine the amount of light transmitted through the spray ($I(x)$ in Eq. 8). The OD image is then reconstructed from the two previous images, using the following equation:

$$\mathrm{OD} = -\ln\frac{I(x)}{I(0)} \tag{11}$$

Figure 4b shows the OD results obtained for the highest fuel injection pressure in the experiments ($P_{\mathrm{inj}} = 4.5$ bars). OD is above 0.8 in the first 5 mm, which corresponds to the primary breakup zone. OD values can reach 0.4 in the secondary breakup zone (between 10 and 20 mm on the Z-axis) and remain below 0.2 in the dilution zone (beyond 20 mm on the Z-axis)

3.2.2 Simulation results

Since the LIF/Mie technique will only be applied in the secondary breakup and dilute zone, two representative simulations are performed in order to quantify multiple scattering (Fig. 5a). Two representative volumes of these two zones are defined and the average representative OD measured in Fig. 4b are applied. The parameters for the simulation are summarized in Table 3:

The optical collection angle of the photons in the simulation is equal to 7° and calculated from the telecentric lens information (No. 5 in Table 1): $f/N = 8$, a field-of-view of 80 mm and a working distance of 226 mm. The results of the simulation are displayed in Fig. 5b, c. For each zone, a map of the distribution of all photons at the output plane is displayed on the left hand and middle side, then the percentage of all the scattering orders observed is represented on the right-hand side. The maps of the distribution of all photons are extracted at a scattering angle of 90° to the laser sheet (the same configuration as the experimental set-up in Fig. 2). Results show that in the secondary breakup zone, single scattering is about 48% and the mean number of scattering events per detected photon is 1.71. By contrast, in the dilute zone, single scattering becomes the dominant process

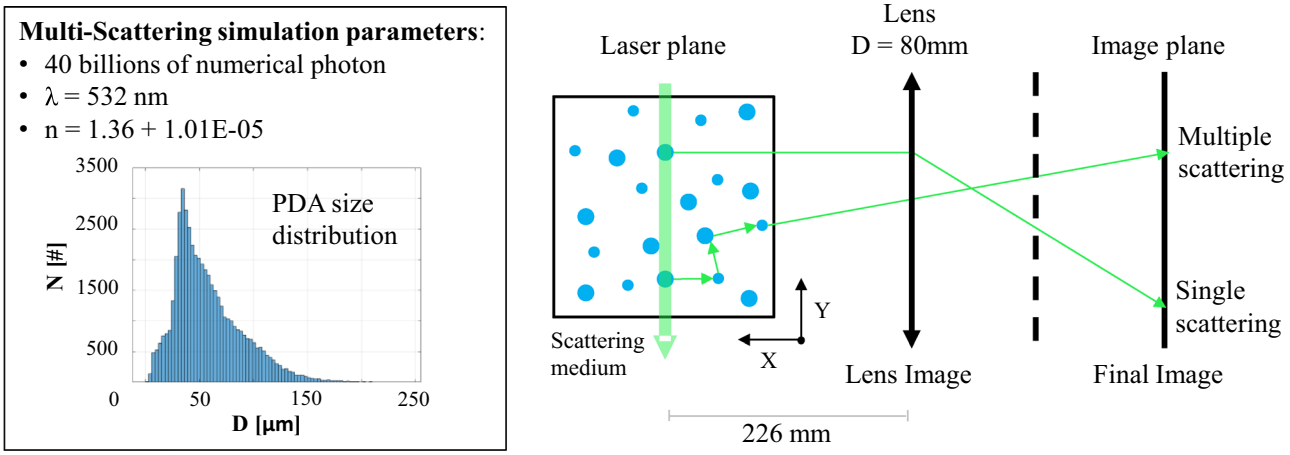

(a) Numerical configuration and parameters

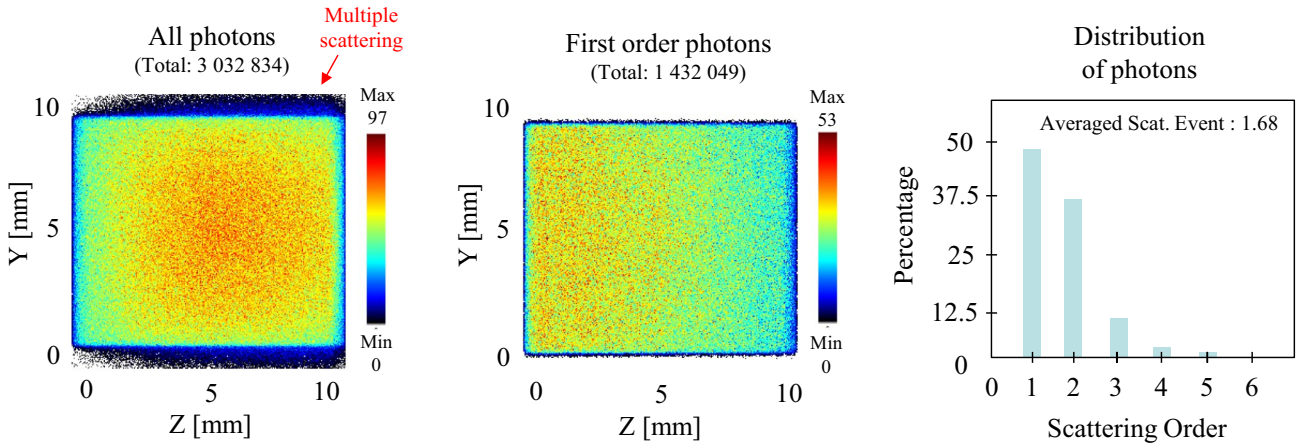

(b) *Results*: Secondary breakup zone (OD = 0.4 & V = 10x10x10 mm^3)

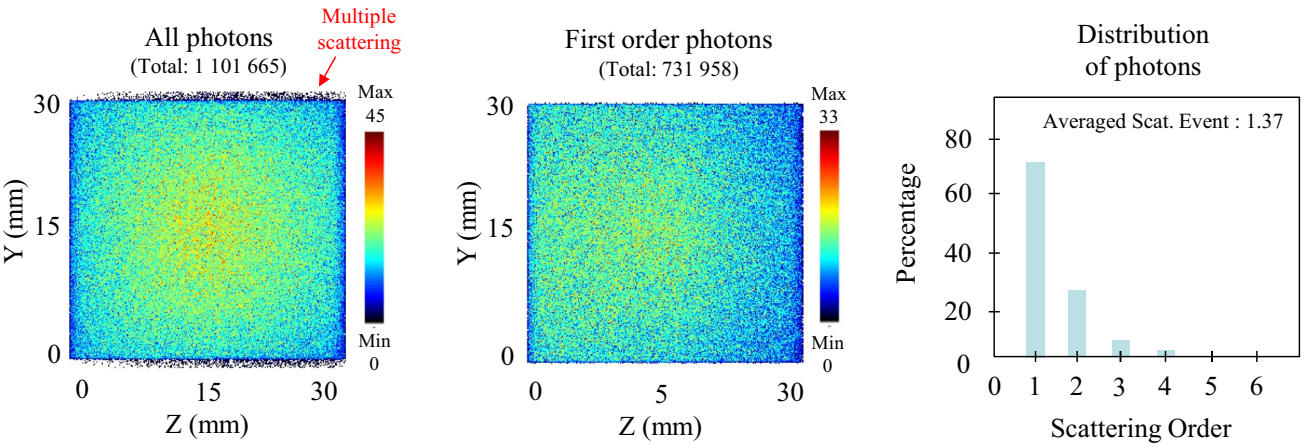

(c) *Results*: Spray region (OD = 0.2 & V = 30x30x30 mm^3)

Fig. 5 **a** Schematic representation of the multiple scattering simulation. Results from the multi-scattering software for different optical conditions: OD = 0.4 (**b**), 0.2 (**c**). For each simulation, $\lambda = 532$ nm, $n = 1.36 + 1.01E{-}05i$ (which corresponds to ethanol seeded with 10 mg/L of Rh6G) and forty billions of numerical photons are released from the light source

Table 3 Parameters for the simulation

Parameters	Secondary breakup zone	Dilute zone
V	$10\times10\times10$ mm^3	$30\times30\times30$ mm^3
OD	0.4	0.2

Table 4 Estimation of the imaginary part of the refractive index given by Eq. 12

Concentration	*k* index
1 mg/L	1.01E–06
10 mg/L	1.01E–05
100 mg/L	1.01E–04

(~ 70%) and multiple scattering reduces significantly (the mean number of scattering events per detected photon is 1.37). According to Berrocal (2006), multiple scattering is negligible until there is a mean of 2 or more scattering events per photon. Additionally, Grosshans et al. (2015) considered that a region of a spray is optically dense when the intensity ratio between the incident light *I (0)* and the transmitted light *I (x)* is less than 37%. In our case, the ratio *I* (x)/*I* (0) exceeds 70% over the entire spray studied. In conclusion, the use of a SLIPI module, allowing the suppression of the effects of multiple scattering in the spray, is therefore not required for the next LIF/Mie measurements under these conditions. In order to limit multiple scattering, observed in the simulation for OD = 0.4 (*Z* = 5–10 mm on Fig. 4), LIF/Mie measurements will be performed from 10 mm from the combustion chamber dome.

4 Analysis of the LIF/Mie technique

In this section, a study of the parameters that influence the LIF and Mie signals is carried out, allowing the possibilities / limitations of the technique to be determined.

4.1 Analysis of the parameters that alter LIF intensity

The fluorescence emission is assumed to be isotropic: intensity does not depend on the viewing angle around the droplet (Coppeta and Rogers 1998). According to Felton et al. (1993), the main parameter that affects the relationship between fluorescence intensity and particle volume is the dye concentration *C* [mol/m^3]. On the one hand, since fluorescent intensity is generally low, it could be tempting to increase the dye concentration. On the other hand, it would correlatively increase the absorption of laser light through the droplet and make the fluorescent intensity no longer proportional to the droplet volume, but to the diameter to a power *F(C)* smaller than 3 (Eq. 12):

$$I_f = I_i k_f \sum n_i D_i^{F(C)} \tag{12}$$

where I_i is the incident light intensity and k_f is a constant that is determined from calibration. To define which concentration of Rh6G has to be used in the experiment, a study on the evolution of *F* as a function of *C* is carried out through the GMLT (generalized Lorenz–Mie Theory) software (Méès and Gouesbet 2001). This software makes it possible to calculate, in the three dimensions of space, the excitation field within an illuminated droplet. In this context, the droplet is considered as a spherical and homogeneous particle. The calculation of the excitation field is performed in the framework of the generalized Lorenz–Mie theory. The input data for this code are the real (*m*) and imaginary (*k*) refractive index, the diameter (*D*) of the droplet, the laser excitation wavelength (λ), the width of the laser beam (*e*), the position of the droplet in the laser beam and the laser polarization (*S*-pol or *P*-pol). The wavelength (532 nm) and the polarization (*P*-pol) used in the simulation are defined by the laser used in the experiments. Then, the droplet is placed at the laser waist (X, Y, Z) = (0, 0, 0) and the half width of the beam is assumed to be infinite. Since the liquid used in the experiments is ethanol, the real part (*m*) of the refractive index is set at 1.36. Since the imaginary part is proportional to the concentration of dye in the liquid, an estimation is made by calculating:

$$k = \frac{\lambda \mu_a}{4\pi} = \frac{\lambda C \varepsilon_a}{4\pi\rho} \tag{13}$$

With λ the excitation wavelength, set at 532 nm, *C* the dye concentration [g/L],ε_a the molar extinction [L/cm*Mol] (set at 113 577 according to Taniguchi et al. (2017)) and ρ the molar mass [g/Mol] (set at 479.01 according to Coplen (1996)). The calculated values of *k* for different dye concentrations are given in Table 4.

Once the laser excitation field is calculated within the droplet, it is spatially integrated over the entire volume of the droplet. This step is then repeated for different particle diameters. The results are available in Fig. 6b. The analysis of the evolution of the fluorescence intensity as a function of the droplet diameter finally makes it possible to estimate the value of the *F* exponent: increasing the dye concentration decreases the value of the exponent *F*. A concentration of 10 mg/L is a good compromise between a sufficiently intense LIF signal, low absorption, and an *F*(*C*) close to 3 (*F* = 2.97). Therefore, in the remainder of the paper, a concentration of 10 mg/L will be used.

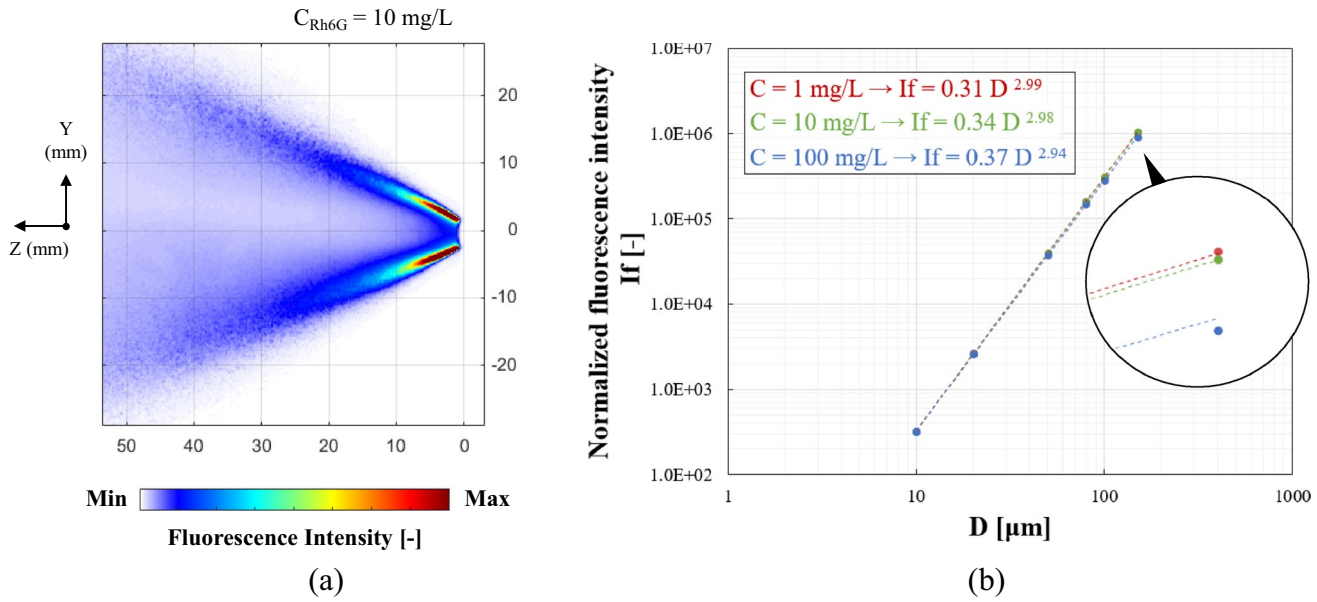

Fig. 6 **a** Average LIF image of the ethanol hollow cone spray, obtained for an injection pressure of $P_{inj} = 3$ bars. The laser sheet propagates from top to bottom. **b** Evolution of fluorescence intensity as a function of particle size for different dye concentrations

4.2 Analysis of the parameters that alter Mie intensity

The fundamental hypothesis given by Yeh et al. (1993), assuming proportionality between the scattered intensity and the droplet square diameter, has been demonstrated to not be valid in practice (Charalampous and Hardalupas, 2011b). Indeed, the scattered intensity I_s depends on the intensity of the light incident on the droplet $I_i(\lambda)$, on the droplet diameter D, on the refractive index of the liquid n and on the scattering angle α. As a result, the proportionality relationship between the scattered intensity and the D^2 is replaced by a diameter to the power M (λ, D, α, n):

$$I_s = I_i k_s \sum n_i D_i^{M(\lambda,D,\alpha,n)} \tag{14}$$

where k_s is a constant that is determined from calibration. Since the parameters λ and n of Eq. 14 are constant in the experiments ($\lambda = 532$ nm and $n = 1.36 + 1.01\text{E}{-}05\text{i}$), the study of the parameters influencing the Mie intensity concerns the scattering angle α and the droplet diameter D.

4.2.1 Influence of the scattering angle

The scattering angle α is defined as the angle between the direction of the light incident on the particle and the detection (or observation) direction. According to the Lorenz–Mie theory (Lorenz 1890; Mie 1908), for a certain droplet diameter (whose size is equivalent to the excitation wavelength), there is a strong dependence between scattered intensity and scattering angle. When using a conventional lens, some variation in scattering angle is observed in the measurement field, making the application of intensimetric measurement difficult. With the LIF/Mie technique, this strong angular dependence cannot be corrected by simply calculating the ratio image because it only affects the Mie signal. A correction approach suggested by Findeisen et al. (2005) consists in generating an image with homogeneously distributed particles and using it as a flat-field image. However, the solution is only applicable if monodisperse seeding is used. An alternative could be to determine the most favorable scattering angle that makes it possible to reduce the intensity variation in the camera field-of-view. Finally, a promising solution to remove this angular dependence is the use of a telecentric lens, which only collects parallel or collimated rays that originate from the laser sheet. Therefore, no angular variation is expected within the field-of-view. To demonstrate the interest of this latter solution, a comparison is made between a conventional lens (No. 4 in Table 1) and a telecentric lens (No. 5 in Table 1) in Fig. 7, under the same experimental conditions (liquid injection pressure of 3 bars and a liquid mass flow-rate of 2.20 g/s).

A mean scattering image of the longitudinal section of the spray is presented in Fig. 7a. This image, obtained with the conventional lens, is not symmetrical about the Z-axis. In fact, an attenuation of approximatively 8% between the maximum amplitudes of the two peaks A and B is observed on a vertical Y-profile at $Z = 15$ mm from the injector ($I_{s(B)} = 92\%\ I_{s(A)}$). In order to understand this result, the main parameters that influence the scattered light intensity I_s will

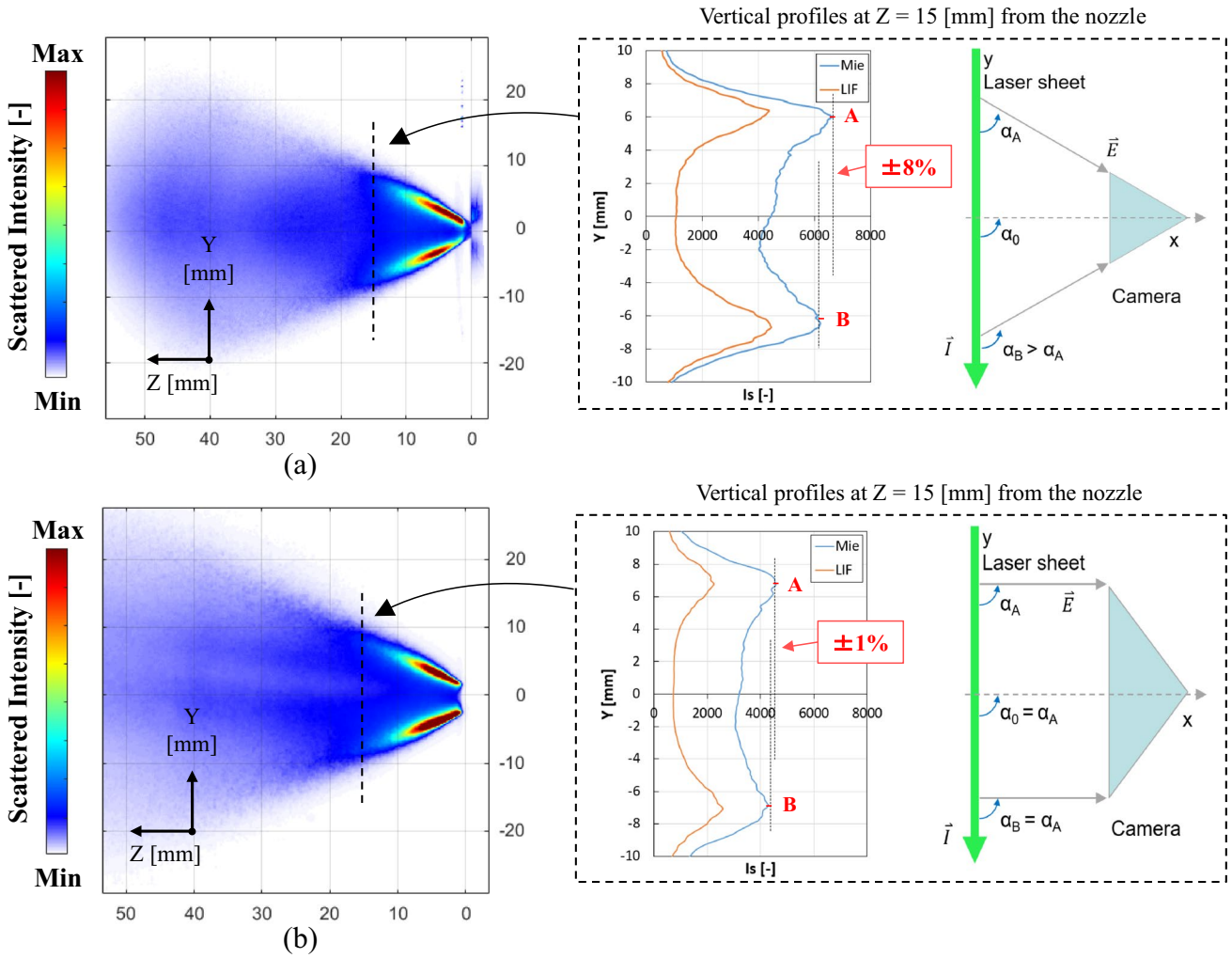

Fig. 7 *Left:* Average Mie scattering image of the ethanol hollow cone spray, obtained for a fuel injection pressure $P_{inj} = 3$ bars. The images are recorded with: **a** Conventional and **b** Telecentric lens. *Right:* Vertical Y-profiles on Mie images at $Z = 15$ mm from the injector and definition of the local scattering angle. The laser sheet propagates from top to bottom

be investigated (Eq. 13). First, the refractive index and the wavelength are constant and can, therefore, be discarded. Second, the LIF profile, shown in Fig. 7a, is symmetrical, implying that the asymmetry is not related to the spray topology. Although not shown here, the diameter profiles measured by PDA are almost symmetrical about the Z-axis (± 1% difference between SMD at points A and B). Third, the laser light extinction through the spray (from A to B) is negligible due to low optical depth (OD < 0.4). Finally, the only factor that may explain the dissymmetry of I_S is a variation of α within the field-of-view. This angular dependence can be quantified by means of MiePlot simulations. Calculations are performed considering a PDA size distribution measured on the edge of the spray (droplet range: 1–150 µm), with a laser wavelength of $\lambda = 532$ nm and the refractive index of ethanol + Rh6G ($C_{Rh6G} = 10$ mg/L $\rightarrow n = 1.36 + 1.01E{-}05i$). Calculations are restricted to a ± 6° range around a scattering angle of 90° because in the experiments with the conventional lens, the scattering angle varies from 84° (top of the image in Fig. 7a) to 96° (bottom of the image in Fig. 7a); and it is equal to 89° and 91° for points A and B, respectively. Simulation results are presented in Fig. 8. The difference in scattered intensity between A and B is roughly equal to 7%, which is similar to the relative intensity drop in the Mie scattering image. In the present experiments, the difference is low due to the small opening angle of the spray (60°), which limits the vertical distance between the two peaks A and B to 12 mm (which corresponds to a 2° angular deviation). For a spray with a larger opening angle (90°), calculations show that the intensity difference between points A and B is about 18%, which would further bias measurements. Benefits of telecentric optics are clearly shown in Fig. 7b, where the intensity profiles on the Mie images are almost symmetrical about the injection axis. A difference of 2%

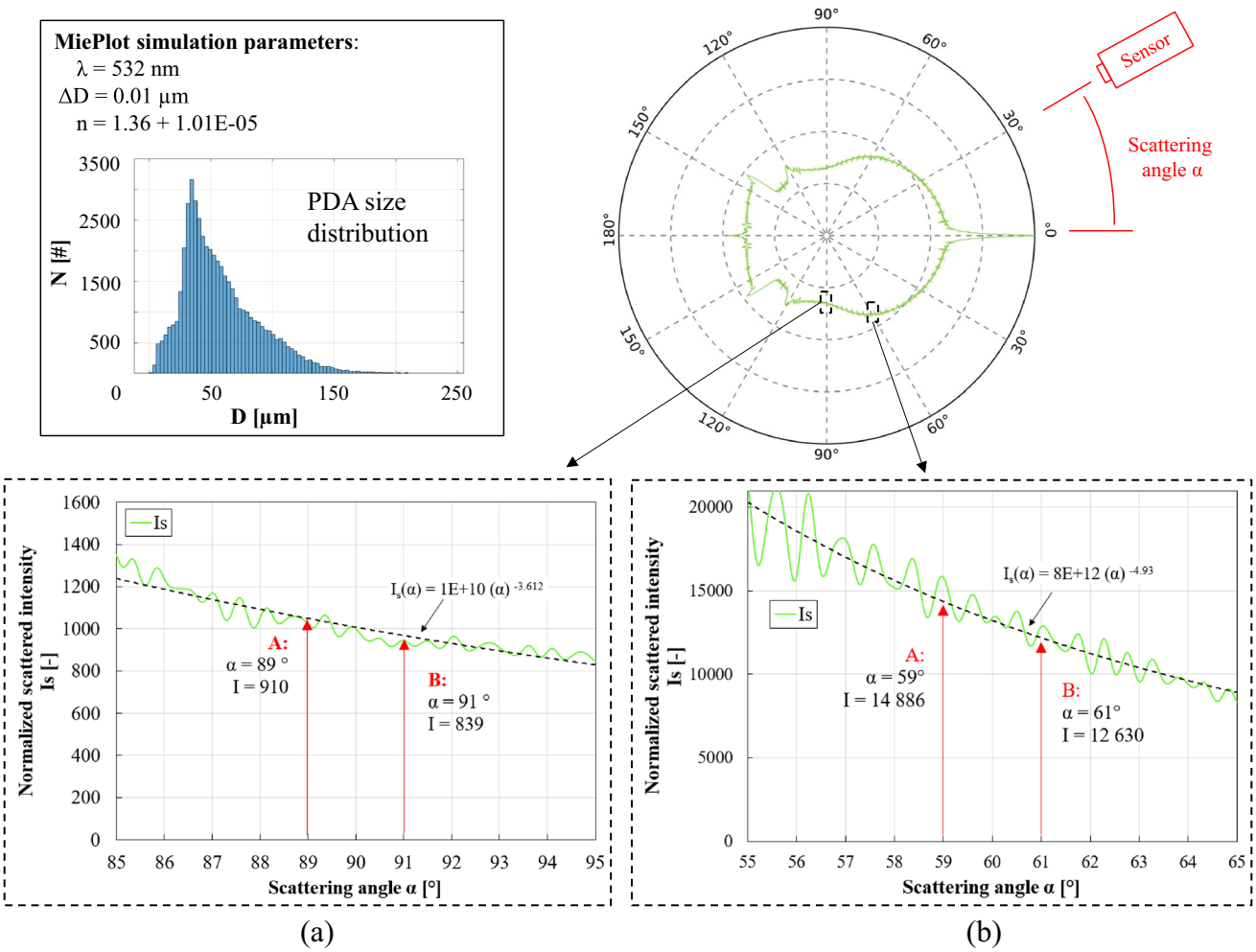

Fig. 8 Evolution of the scattered intensity as a function of the scattering angle, in the range [1–150] µm. Curve **a** is defined for an observation angle between the lens and the measurement plane of 90°, while curve **b** represents an observation angle of 60°. A and B represent the positions of the two peaks presented in Fig. 7. The intensity decrease is significantly higher: 16% at a mean scattering angle of 60° and 7% at 90°

is observed between points A and B, which is similar to the small dissymmetry observed in the PDA results. The slight remaining dissymmetry originates from other physical phenomena intrinsic to the spray or the injector (e.g., manufacturing tolerances).

The inaccuracy of droplet sizing using a conventional lens is proportional to the variation of the Mie intensity signal between both edge of the image, resulting from the local scattering angle imposed by the lens. It has to be noted that this phenomenon is not present when using a telecentric lens (θ is fixed at 90°). Owing to these good results, the use of the telecentric lens has been retained in the experiments presented hereafter. The telecentric lens has a fixed working distance of 227 mm.

4.2.2 Influence of the droplet diameter

The last parameter that affects the relationship between the scattered intensity and the droplet surface is the droplet diameter D. According to Charalampous and Hardalupas (2011b), in the range of interest 1–150 µm, the D^2 law is invalidated and the M exponent steadily decreases. In addition, recent work conducted by Koegl et al. (2022) has shown that the polarization of the incident light influences the proportionality between Mie signal and droplet diameter, which therefore influences the sensitivity of the LIF/Mie results. Previous work carried out by Hofeldt (1993a, 1993b) has highlighted that perpendicular polarization (s-pol) is proportional to the square of diameter D^2, while parallel polarization (p-pol) is proportional to the diameter D. With these considerations, Stiti et al. (2023) have developed a new

method combining SLIPI and polarization ratio method to measure the D_{21} field in an optically dense spray.

In order to quantify this impact of droplet diameter and incident polarization on M exponent, a numerical study is carried out through the MiePlot software (Laven 2008). Simulations are performed on monodisperse droplets with diameters ranging from 1 to 150 µm. The input data for the calculation consider here again a laser wavelength of $\lambda = 532$ nm, a refractive index of $n = 1.36 + 1.01\text{E}{-}05\text{i}$ (ethanol + 10 mg/L of Rh6G), and a scattering angle of 90°. The calculation is made for a diameter increment of $\Delta D = 0.05$ µm. The results obtained confirm first the observations reported in the literature, i.e., the s-pol signal is nearly proportional to D^2 ($M = 1.9032$), while the p-pol signal is nearly proportional to D ($M = 0.9131$), in the range of interest: 1–150 µm (Fig. 9a). For this reason, *s*-pol seems essential when measuring SMD with LIF/Mie technique. Figure 9b shows different trends depending on the diameter range: for 1–30 µm, the value of the M is 1.723, for 30–100 µm, the value of the M is close to 2.03, and for 10–150 µm, the value of the M is close to 2. Based on this observation, it becomes evident that the particle diameter significantly impacts the M exponent. Consequently, applying a single exponent across a broad range of diameters, such as 1–150 µm, proves challenging. Finally, the determination of the F and M exponents shows that the LIF/Mie is not proportional to a diameter:

$$\text{SMD}^{\text{PDA}} = \frac{\sum_i^N D^3}{\sum_i^N D^2} \text{has the unit of a diameter} \tag{15}$$

$$\frac{\text{LIF}}{\text{Mie}} = \frac{\sum_i^N D^F}{\sum_i^N D^M} = \frac{\sum_i^N D^{2.97}}{\sum_i^N D^{1.90}} \text{has the unit of a diameter to a power of 1.07} \tag{16}$$

To overcome this bias, the most straightforward method consists in applying a calibration on LIF/Mie, which will be described in the next section.

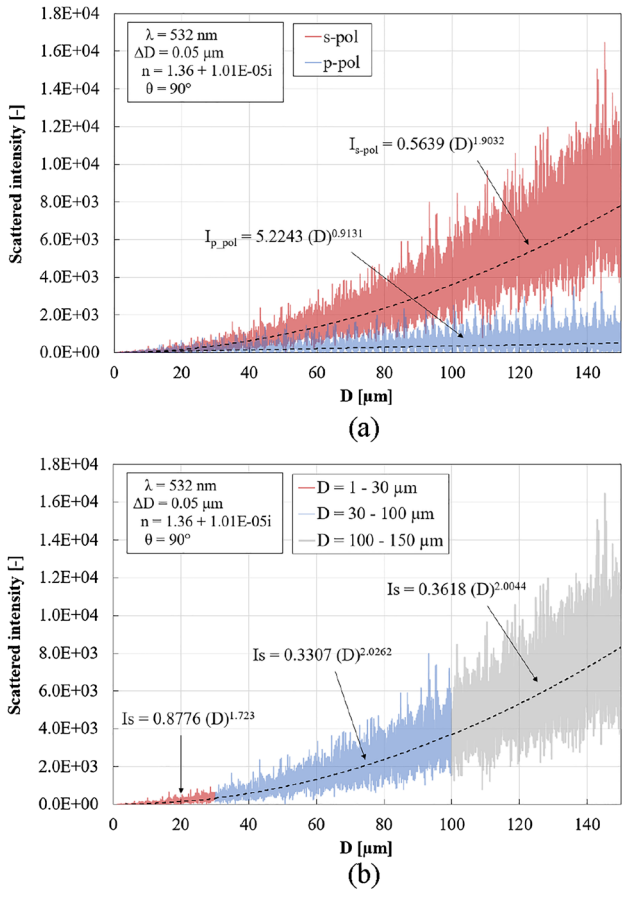

Fig. 9 Simulation of the Mie scattered signals, *s*-pol and *p*-pol as a function of droplet diameter, in a case of monodisperse size distribution ($\lambda = 532$ nm, $m = 1.36 + 1.01\text{E}{-}05\text{i}$, $\theta = 90°$)

5 Droplet size characterization

5.1 LIF/Mie calibration

In the literature, different methods are used. For example Domann and Hardalupas (2003), Charalampous and Hardalupas (2004), and Charalampous and Hardalupas (2011a) have carried out theoretical analysis to correct the proportionality error: First, a droplet size distribution is defined using a distribution function (e.g., Rosin–Rammler), and the corresponding scattered and fluorescent light is calculated with the Lorenz–Mie theory. Second, LIF and Mie measurements are compared with the simulations. Finally, a proportionality coefficient is defined numerically and applied to the LIF/Mie. Domann and Hardalupas (2003) made comparisons between SMD results from the LIF/Mie technique (calibrated by theoretical analysis) and PDA, showing a 10% sizing error. Mishra et al. (2017a, 2017b), Koegl et al. (2018a, 2018b) or even Koegl et al. (2018a, 2018b) performed a calibration using a monodisperse droplet generator that accurately controls the droplet diameter in the range of interest. LIF and Mie signals from the droplets are sequentially recorded as a function of droplet diameter. The correlation between LIF/Mie intensity and droplet diameter is then used for the calibration of the LIF/Mie. The major disadvantage of

this method is that a monodisperse injection system must be added to the experiments and the optical set-up must be adapted to a much smaller field-of-view. Sankar et al. (1999) and Le Gal et al. (1999) have developed a look-up table (LUT) to relate the values of SMD measured with a PDA system and the LIF/Mie ratios deduced from image processing at the same points. The method is effective, but the only drawback is the requirement of a second optical diagnostic technique. In this paper, we have chosen to use PDA calibration, because this technique is considered as a reference for accurate droplet sizing. Moreover, PDA results are also used to make comparisons with LIF/Mie SMD measurements.

In the literature, many studies have shown that the LIF intensity of certain dyes exhibits a temperature dependence (Coppeta and Rogers 1998; Chaze et al. 2016; Doublet et al. 2019). As a result, when using a temperature-dependent dye, there should be as many calibration curves as temperatures. However, in this paper, the dye used (Rh6G) is almost independent of temperature: temperature sensitivity equal to −0.07%/°C (Doublet et al. 2019). Moreover, it is also well-known that that ethanol evaporation affects dye concentration (Koegl et al. 2020) in the droplet volume, which may bias LIF/Mie ratio measurements. Calculations of droplet vaporization using the classical D^2 law were performed and indicate that in our experiments, the droplet volume remains practically unchanged from right to left on the images, and that the dye concentration is unaffected.

Figure 10 presents LIF, Mie and LIF/Mie average maps recorded for an injection pressure of $P_{inj} = 3$ bars. Building the calibration table over the largest possible diameter range requires PDA measurements to be performed at several distances from the injector ($Z = 20$–30 mm) and for different injection pressures ($P_{inj} = 1.5$ & 3 bars). For each pressure, measurements are realized on line segments, perpendicular to the spray axis (Fig. 11a), along which mean diameter has the highest spatial gradient. Intensity profiles are considered at the same Z distances on the LIF/Mie image and a cloud of experimental points can be plotted (Fig. 11b). For a given LIF/Mie, oscillations of diameter values are observed, which may be attributed to the coherence length of laser radiation that can generate interferences in Mie scattering. Indeed, as reported in the literature (Van de Hulst 1981; Bohren and Huffman

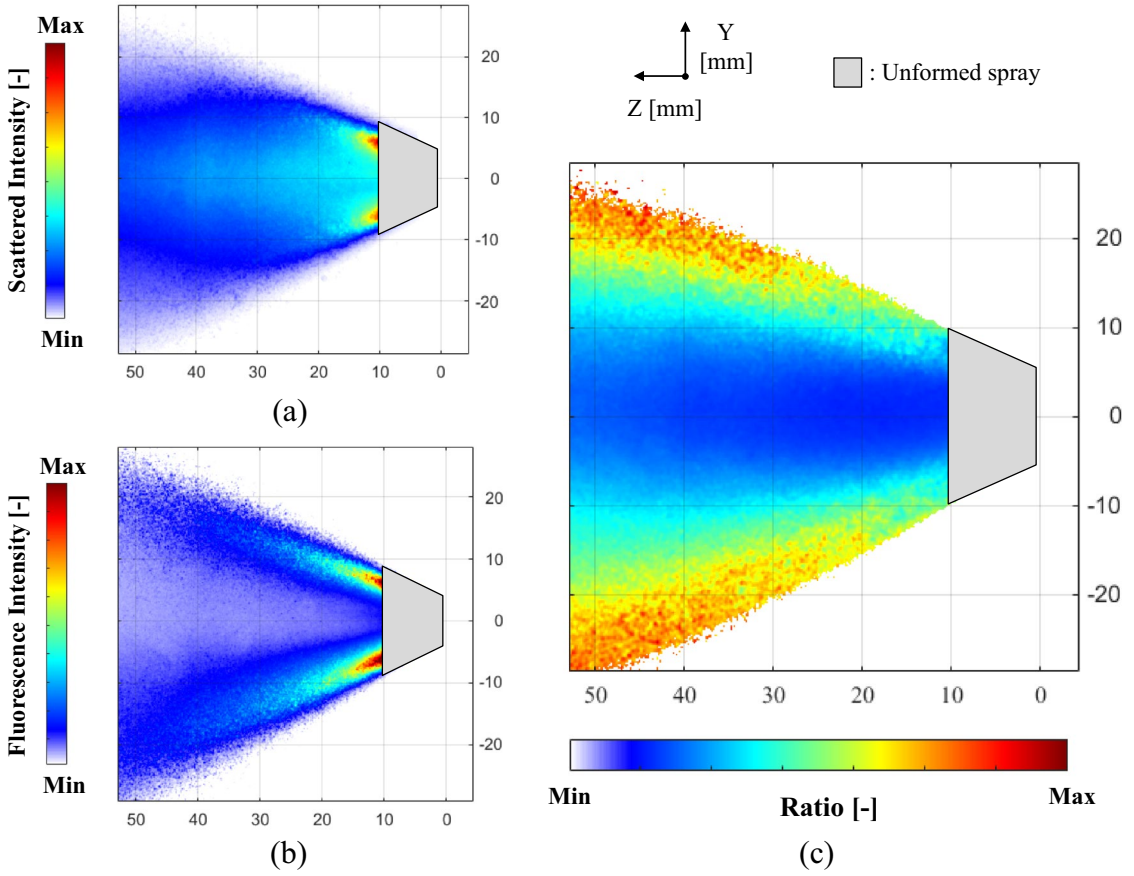

Fig. 10 Average **a** Mie, **b** LIF and **c** LIF/Mie maps of the ethanol hollow cone spray, obtained for an injection pressure of $P_{inj} = 3$ bars. The laser sheet propagates from top to bottom

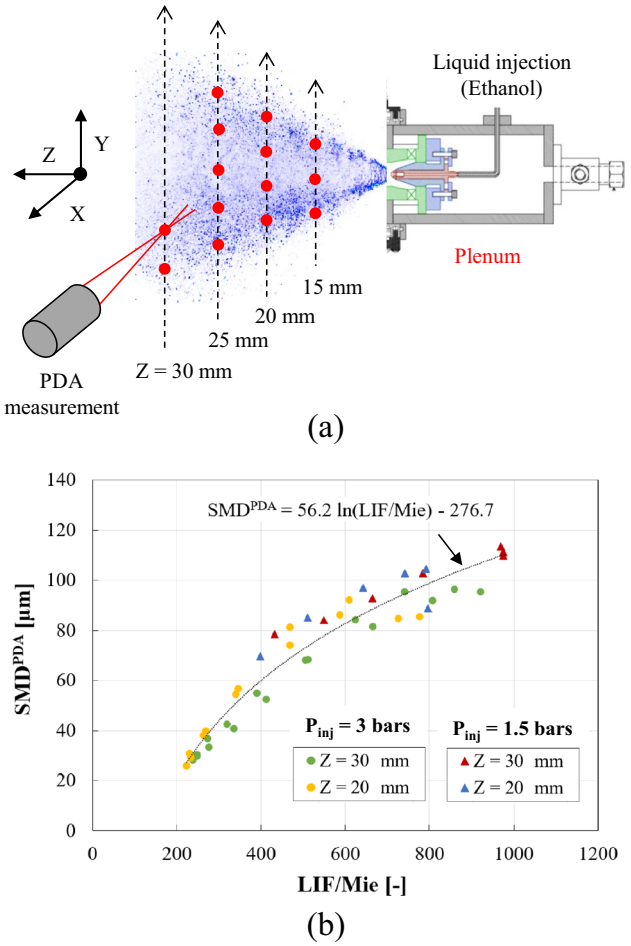

Fig. 11 **a** Positions of the PDA measurement volume at different distances (Z=15, 20, 25 and 30 mm) from the injector. **b** LUT correlating LIF/Mie ratios to SMD measured by PDA. In order to scan a maximum diameter range, the data are derived from two injection pressures (P_{inj}=1.5 & 3 bars) and two distances from the injector (Z=20 & 30 mm)

1983), the interaction of electromagnetic waves with droplets results in various scattering orders. As shown by Albrecht et al. (2003), Bakic (2009), in the far field, waves from the different scattering orders interfere and cause the characteristic angular intensity distribution of the exhibiting scattering lobes. Further investigations have shown that for ultra-short lasers [fs], the coherence length can be smaller than droplet diameters (Albrecht et al. 2003), which eliminates intensity fluctuations in the far field. However, the present experiments use a Nd: YAG laser with a 10 ns pulse, which results in the significant standard deviation observed on the LIF/Mie. In addition, the scattering of the results may also be attributed to low values of LIF signal, leading to low SNR values. For example, the uncertainty on the SMD is ± 5 µm for a LIF/Mie equal to 250 and increases to ± 15 µm for a LIF/Mie equal to 800 (Fig. 11b). As shown in Fig. 11b, a logarithmic law can be used to build the LUT to transform LIF/Mie images into SMD maps.

5.2 Quantitative measurements of droplet size

In this section, the LIF/Mie technique is applied for quantitative measurements of droplet size in a hollow cone spray, at different injection pressures. Figure 12 represents different SMD maps obtained by applying the LUT on LIF/Mie maps. As mentioned previously, the first 10-mm downstream from the injector are not considered when calculating SMD values, because droplets have not yet formed in this spray region. At first sight, it is obvious that the spray is not perfectly symmetrical around the injector axis; larger droplets are present in the lower part of the spray. Although the laser sheet propagates from top to bottom on the spray image, no systematic signal extinction is visible along that direction on both LIF and Mie images. This suggests that there must be other physical reasons in the spray formation process that lead to the asymmetry, as mentioned previously. In Fig. 12a for an injection pressure of P_{inj} = 1.5 bars, the spray does not yet appear to be formed, because the hollow cone representative of this type of injector is not apparent. Between 10 and 20 mm, the SMD varies from a minimum of about 50 µm in the center to a maximum of 100 µm at the edges. Since the spray is not completely open, between 30 and 50 mm, droplets from the top and the bottom mix together, which increases the SMD to approximately 75 µm in the center. In Fig. 12b for an injection pressure of P_{inj} = 3 bars, the spray seems to have reached its optimum opening angle of 60°. The hollow cone clearly appears and the SMD varies between a minimum value of 30 µm in the center and a maximum of 110 µm at the edges. In Fig. 12c for an injection pressure of P_{inj} = 4.5 bars, the spray is well-formed, and the hollow cone is even more apparent. The spray looks almost symmetrical. The SMD varies between a minimum of about 20 µm in the center and a maximum of 110 µm at the edges. Validation of these results is performed by comparing SMD values deduced from the LIF/Mie image processing with those obtained by PDA measurements. The results are shown in Fig. 13. The comparison is carried out at Z distances different from those used to construct the calibration table: Z = 15 and 25 mm. A good match between measurements is observed, both at the edges and at the center of the spray.

6 Conclusions

In this paper, the LIF/Mie technique was investigated experimentally and theoretically, on an ethanol hollow cone spray generated by a pressure swirl atomizer, using an innovative optical set-up including a TwinCam system and a telecentric

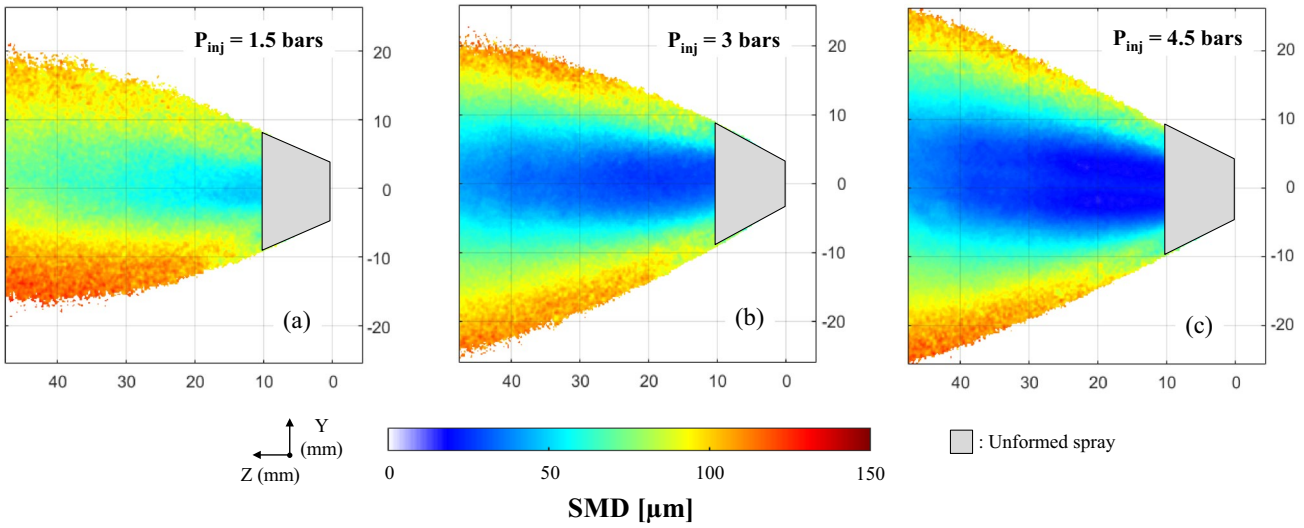

Fig. 12 Average SMD mappings (over 800 images) of the ethanol hollow cone spray, obtained for different injection pressures: **a** $P_{inj}=1.5$ bars, **b** $P_{inj}=3$ bars and **c** $P_{inj}=4.5$ bars

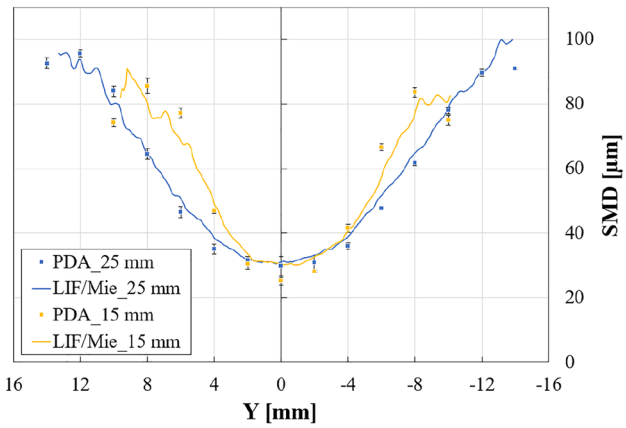

Fig. 13 Comparison between PDA and LIF/Mie SMD measurements, for two injector distances ($Z=15$ and 25 mm) at $P_{inj}=3$ bars

lens. The TwinCam system allows the physical superimposition of the optical paths and simplifies the ratio measurement by contrast to set-ups used in the literature. Experiments and simulations first showed that the optical conditions imposed by the spray do not prevent the application of the technique (i.e., low laser attenuation and limited multiple scattering). The parameters influencing the Mie and LIF images were then analyzed, and the results showed that the assumptions of proportionality between fluorescence/scattering intensity and volume/surface droplet are not valid in the present spray. The present paper shows that the telecentric lens, which only collects light parallel to the optical axis, makes it possible to remove the angular dependence of the Mie signal on the images. Moreover, the diameter of the particles strongly influences the M exponent, and it is difficult to apply a single exponent over a wide range of diameters. To overcome this dependence, a calibration of LIF/Mie, based on the use of a LUT, was also implemented to relate the SMD measured by PDA and the LIF/Mie. The technique was then applied to study the influence of various parameters on droplet size in the spray, and the comparison between PDA measurements and LIF/Mie obtained by LUT shows a good agreement with an uncertainty close to 12%. Finally, the study demonstrates the strong capability of the LIF/Mie technique for further industrial applications with two outstanding advantages compared to point-measurement techniques: a whole map is available with a high spatial resolution and within a reasonable time. The next work will be to apply the technique to denser sprays where the use of the SLIPI device is necessary.

Acknowledgements The authors gratefully acknowledge ONERA and "Région Occitanie" for PhD funding support. The authors would also like to thank ONERA's manufacturing workshop for their practical assistance, without which the experiments in this paper could not have been carried out.

Author contributions SG wrote the manuscript text, generated figures, and was the primary contributor to the measurement system development. PD, CL, and MO oversaw the study conception and design. MS and GI contributed to the development of the measurement system. EB contributed to the Monte Carlo simulation. All authors contributed to the field experiments and reviewed the manuscript.

Funding This work was supported by ONERA and "Région Occitanie."

Data availability The data that support the findings of this study are available from the corresponding author, S. Garcia, upon reasonable request.

Declarations

Conflict of interest The authors declare no conflicts of interest.

References

Albrecht HE, Borys M, Damaschke N, Tropea C (2003) Laser doppler and phase doppler measurement techniques. Springer-Verlag Berlin, Heidelberg

Bakic S (2009) Time integrated detection and applications of fs-laserpulses scattered by small particles, PhD Thesis. Technische Universitat Darmstadt

Berrocal E et al (2008) Application of structured illumination for multiple scattering suppression in planar laser imaging of dense sprays. Opt Express 16:17870–17881

Berrocal E, Kristensson E, Zigan L (2018) Light sheet fluorescence microscopic imaging for high-resolution visualisation of spray dynamics. Int J Spray Combust Dyn 10(1):86–98

Berrocal E et al (2019) Two-photon fluorescence laser sheet imaging for high contrast visualization of atomizing sprays. OSA Contin 2(3):983–993

Berrocal E (2006) Multiple scattering of light in optical diagnostics of dense sprays and other complex turbid media. Cranfield University, Cranfield

Berrocal E et al. (2023) Optical spray imaging diagnostics. Aaerospace Research Central.

Bohren C, Huffman D (eds) (1983) Absorption and scattering of light by small particles. Wiley, New York

Charalampous G and Hardalupas Y (2004) In:Optimisation of the droplet sizing accuracy of the combined scattering (MIE)/laser induced fluorescence (LIF) technique. In: 20th international symposium on apply of laser techniques to fluid mechanics. Lisbon, Portugal

Charalampous G, Hardalupas Y (2011) Method to reduce errors of droplet sizing based on the ratio of fluorescent and scattered light intensities. Appl Opt 50:3622–3637

Charalampous G, Hardalupas Y (2011) Numerical evaluation of droplet sizing based on the ratio of fluorescent and scattered light intensities (LIF/MIE technique). Appl Opt 50:1197–1209

Chaze W, Caballina O, Castanet G, Lemoine F (2016) The saturation of the fluorescence and its consequences for laser-induced fluorescence thermometry in liquid flows. Exp Fluids. https://doi.org/10.1007/s00348-016-2142-8

Coplen TB (1996) Atomic weights of the elements 1995. Pure Appl Chem 68(12):2339–2359

Coppeta J, Rogers C (1998) Dual emission laser induced fluorescence for direct planar scalar behavior measurements. Exp Fluids 25:1–15

Domann R, Hardalupas Y (2001) A study of parameters that influence the accuracy of the planar droplet sizing (PDS) technique. Part Part Syst Charact 18:3–11

Domann R, Hardalupas Y (2003) Quantitative measurement of planar droplet sauter mean diameter in sprays using planar droplet sizing. Part Part Syst Charact 20:209–218

Doublet P et al (2019) Saturated laser induced fluorescence in liquid kerosene seeded with a dye: influence of temperature and excitation intensity. Appl Phys. https://doi.org/10.1007/s00340-019-7299-4

Felton PG, Bracco FV, Bardsley MEA (1993) On the quantitative application of exciplex fluorescence to engine sprays. J Eng 103:1254–1262

Findeisen J et al. (2005) 2D concentration measurements based on Mie scattering using a commercial PIV system. In: 6th international symposium on particle image velocimetry, Pasadena

Frantz D, Jönsson J, Berrocal E (2022) Multi-scattering software: part II: experimental validation for the light intensity distribution. Opt Express 30(2):1261–1279

Grosshans H, Kristensson E, Szasz R-Z, Berrocal E (2015) Prediction and measurement of the local extinction coefficient in sprays for 3D simulation/experiment data comparison. Int J Multiph Flow 72:218–232

Hervo L, Senoner J, Biancherin A, Cuenot B (2018) Large-Eddy simulation of kerosene spray ignition in a simplified aeronautic combustor. Flow Turbul Combust 101:603–625

Hofeldt DL (1993) Full-field measurements of particle size distributions II: experimental comparison of the polarization ratio and scattered intensity methods. Appl Opt 32(36):7559–7567

Hofeldt DL (1993) Full-field measurements of particle size distribution: I. Theorical limitations of the polarization ratio method. Appl Opt 32(36):7551–7558

Jermy MC, Allen A (2002) Simulating the effects of multiple scattering on images of dense sprays and particle fields. Appl Opt 41(20):4188–4196

Jermy MC, Greenhalgh DA (2000) Planar drop sizing by elastic and fluorescence scattering in sprays too dense for phase Doppler measurement. J Appl Phys 86:71703–71710

Jönsson J, Berrocal E (2020) Multi-scattering software: part I: online accelerated Monte Carlo simulation of light transport through scattering media (https://multi-scattering.com). Opt Express 28(25): 37612–37638

Koegl M et al (2018) Analysis of ethanol and butanol direct-injection spark-ignition sprays using two-phase structured laser illumination planar imaging droplet sizing. Int J Spray Combust Dyn 11:1–16

Koegl M, WeiB C, Zigan L (2020) Fluorescence spectroscopy for studying evaporating droplets using the dye eosin-Y. Sensors 20(21):59–85

Koegl M et al (2022) Polarization-dependent LIF/Mie ratio for sizing of micrometric ethanol droplets doped with Nile red. Appl Opt 61(14):4204–4214

Koegl M et al. (2018) 3D LIF/Mie planar droplet sizing in IC engine sprays using single-droplet calibration data. 14th ICLASS, Chicago

Kristensson E, Berrocal E, Richter M, Aldén M (2010a) Nanosecond structured laser illumination planar imaging for single-shot imaging of dense sprays. Atom Sprays 20:337–343

Kristensson E et al (2010b) Structured illumination for 3-D Mie imaging and 2-D attenuation measurements in optically dense sprays. Proc Combust Inst 33:855–861

Kristensson E, Berrocal E, Alden M (2011) Extinction coefficient imaging of turbid media using dual structured laser illumination planar imaging. Opt Lett 36(9):1656–1658

Kubin R, Fletcher A (1982) Fluorescence quantum yields of some rhodamine dyes. J Lumin 27:455–462

Laven P (2008) Simulation of rainbows, coronas, and glories by use of Mie theory. Appl Opt 42(3):436–444

Le Gal P, Farrugia N, Greenhalgh D-A (1999) Laser sheet dropsizing of dense sprays. Opt Laser Technol 31(1):75–83

Lefebvre AH, McDonell VG (2017) Atomization and sprays. CRC Press Taylor & Francis Group, Boca Raton

Lorenz L (1890) Lysbevaegeisen i og uden for en hal plane lysb olger belyst kluge. Vidensk, Selk Skr 6:1–62

Méès L, Gouesbet G (2001) Time-resolved scattering diagrams for a sphere illuminated by plane wave and focused short pulses. Opt Commun 194:59–65

Mie G (1908) Beitrage zur optik trubermedien, speziell kolloidaler etallosungen. Annalen Physik 25:377–452

Mishra Y, Kristensson E, Berrocal E (2014) Reliable LIF/MIE droplet sizing in sprays using structured laser illumination planar imaging. Opt Express 22:4480–4492

Mishra YN et al (2017) 3D mapping of droplet sauter mean diameter in sprays. Appl Opt. https://doi.org/10.1364/AO.58.003775

Mishra Y et al (2017) Comparison between two-phase and one-phase SLIPI for instantaneous imaging of transient sprays. Exp Fluids. https://doi.org/10.1007/s00348-017-2396-9

Mugele R, Evans HD (1951) Droplet size distribution in sprays. Ind Eng Chem 43:1317–1324

Rayleigh L (1878) On the instability of jets. Proc Lond Math Soc 10:4–12

Sanjosé M et al (2011) Fuel injection model for Euler-Euler and Euler-Lagrange large-eddy simulations of an evaporating spray inside an aeronautical combustor. Int J Multiph Flow 37(5):514–529

Sankar SV, Mahleret KE, Robart DM (1999) Rapid characterization of fuel atomizers using an optical patternator. J Eng Gas Turbines Pow 121:409–414

Stiti M et al (2023) Droplet sizing in atomizing sprays using polarization ratio with structured laser illumination planar imaging. Opt Lett 48(15):4065–4068

Stiti M, Lehnert B, Wensing M, Berrocal E (2022) Multiple scattering suppression for correct light transmission measurements through the ECN Spray G running with ethanol. In: 31th conference on liquid atomization and spray systems (Virtual) Tel-Aviv, IS, ILASS

Stojkovic B-D, Sick V (2001) Evolution and impingement of an automotive fuel spray investifated with simultaneous LIF/Mie techniques. J Appl Phys 73:75–83

Taniguchi M, Du H, Lindsey JS (2017) PhotochemCAD 3: diverse modules for photophysical calculations with multiple spectral databases. Photochem Photobiol 94(2):277–289

Van de Hulst H (ed) (1981) Light scattering by small particles. Dover, Illinois

Wellander R et al (2011) Three-dimensional measurement of the local extinction coefficient in a dense spray. Meas Sci Technol. https://doi.org/10.1088/0957-0233/22/12/125303

Yeh C, Kosaka H, Kamimoto T (1993) A fluorescence / scattering imaging technique for instantaneous 2D measurement of particle size distribution in a transient spray. Opt Part Sizing 93:4008–4013

Ying L et al (2007) Fluorescence spectrum characteristic of ethanol–water excimer and mechanism of resonance energy transfer. Chin Phys 16(5):1300–1307